Resource

Cell

DNA Demethylation Dynamics in the Human Prenatal Germline

Graphical Abstract

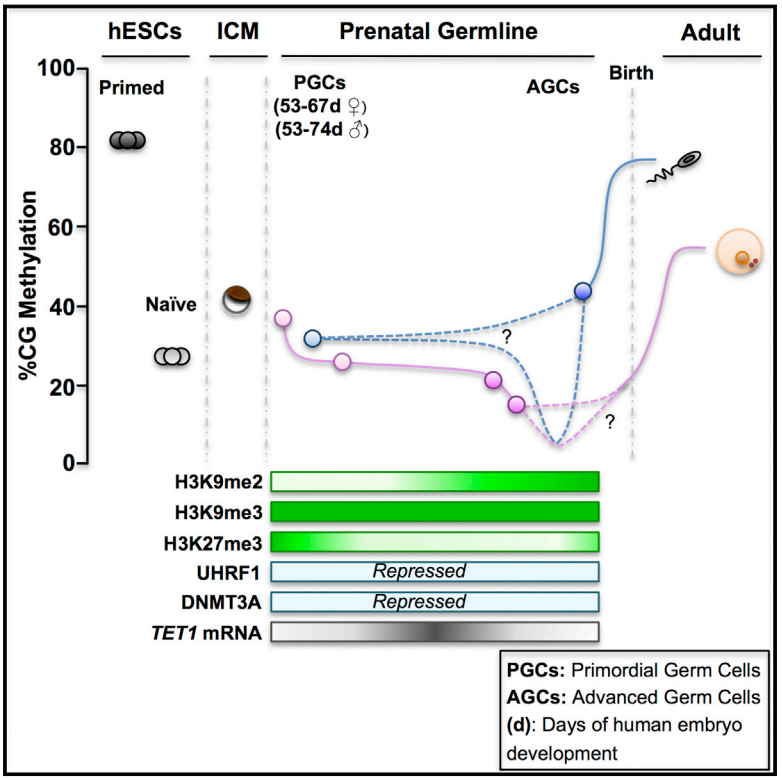

Highlights

- Single-base-resolution methylome resource for human prenatal germline cells
- Comprehensive transcriptional resource for human prenatal germline cells
- Human germline is distinct from inner cell mass and naive pluripotent stem cells
- Naive human pluripotent stem cells have hotspots of unbridled DNA demethylation

Authors

Sofia Gkountela, Kelvin X. Zhang, ..., Pao-Yang Chen, Amander T. Clark

Correspondence

paoyang@gate.sinica.edu.tw (P.-Y.C.), clarka@ucla.edu (A.T.C.)

In Brief

DNA methylome and transcriptome have been profiled in developing prenatal germline cells, and global changes in gene expression do not correlate with global changes in DNA methylation.

Accession Numbers

GSE63392
GSE63393

Gkountela et al., 2015, Cell *161*, 1425–1436
June 4, 2015 ©2015 Elsevier Inc.
http://dx.doi.org/10.1016/j.cell.2015.05.012

Resource

Cell

DNA Demethylation Dynamics in the Human Prenatal Germline

Sofia Gkountela,[1] Kelvin X. Zhang,[2] Tiasha A. Shafiq,[1] Wen-Wei Liao,[6] Joseph Hargan-Calvopiña,[1] Pao-Yang Chen,[6,7,*] and Amander T. Clark[1,2,3,4,5,7,*]

[1]Department of Molecular Cell and Developmental Biology
[2]Department of Biological Chemistry
[3]Eli and Edythe Broad Center of Regenerative Medicine and Stem Cell Research
[4]Jonsson Comprehensive Cancer Center
[5]Molecular Biology Institute
University of California, Los Angeles, Los Angeles, CA 90095, USA
[6]Institute of Plant and Microbial Biology, Academia Sinica, Taipei 11529, Taiwan
[7]Co-senior author
*Correspondence: paoyang@gate.sinica.edu.tw (P.-Y.C.), clarka@ucla.edu (A.T.C.)
http://dx.doi.org/10.1016/j.cell.2015.05.012

SUMMARY

Global DNA demethylation in humans is a fundamental process that occurs in pre-implantation embryos and reversion to naive ground state pluripotent stem cells (PSCs). However, the extent of DNA methylation reprogramming in human germline cells is unknown. Here, we performed whole-genome bisulfite sequencing (WGBS) and RNA-sequencing (RNA-seq) of human prenatal germline cells from 53 to 137 days of development. We discovered that the transcriptome and methylome of human germline is distinct from both human PSCs and the inner cell mass (ICM) of human blastocysts. Using this resource to monitor the outcome of global DNA demethylation with reversion of primed PSCs to the naive ground state, we uncovered hotspots of ultra-low methylation at transposons that are protected from demethylation in the germline and ICM. Taken together, the human germline serves as a valuable in vivo tool for monitoring the epigenome of cells that have emerged from a global DNA demethylation event.

INTRODUCTION

Genome-wide DNA demethylation is essential in the pre-implantation embryo and in the prenatal germline to prevent the heritable transmission of abnormal cytosine methylation (epialleles) from parent to child (Heard and Martienssen, 2014). In the pre-implantation embryo, this involves removal of the cytosine methylation acquired in the parental gametes prior to fertilization. In the prenatal germline, this involves removing cytosine methylation in primitive germline cells called primordial germ cells (PGCs), the precursors of eggs and sperm. The dynamics of DNA demethylation during these two periods has been extensively studied in the mouse, with DNA methylation reaching the lowest point during PGC development at embryonic day 13.5 (E13.5) of mouse gestation. At this time point, less than 10% of cytosines in a CpG sequence context remain methylated in genomic DNA (Seisenberger et al., 2012; Kobayashi et al., 2013; Wang et al., 2014b). Therefore, E13.5 of mouse PGC development is often referred to as the germline epigenetic ground state (Hajkova, 2011).

In vitro, DNA demethylation occurs when primed human embryonic stem cells (hESCs) and serum-grown mouse ESCs are reset to the naive ground state (Habibi et al., 2013; Ficz et al., 2013; Takashima et al., 2014). In humans, converting primed hESCs to the naive ground state causes more than a 50% reduction in CpG methylation, together with the removal of non-CpG methylation (Takashima et al., 2014). It is unknown whether loss of CpG methylation in naive ground state of human pluripotent stem cells resembles the hypomethylated state of the human inner cell mass (ICM) or possibly the methylation of human germline cells.

In humans, the dynamics of cytosine demethylation in pre-implantation embryos shares tremendous similarity with mouse embryos of the equivalent stage (Smith et al., 2014; Guo et al., 2014). However, a distinction between the two species occurs at transposons and, in particular, the long interspersed nuclear element (LINE) subfamilies in which DNA sequence differs substantially between the two species (Smith et al., 2014; Guo et al., 2014). Even though pre-implantation embryos are considerably hypomethylated relative to the gametes from which they originate, there remains significant CpG methylation in the ICM of both species, leading to the hypothesis that, similar to the mouse, the bulk of DNA demethylation during development in vivo occurs in the germline.

In humans, there is limited information on the dynamics of DNA demethylation in the germline during prenatal life, except for immunofluorescence studies revealing that the germline is globally hypomethylated from at least 42 days post-fertilization (Gkountela et al., 2013). To determine whether the human germline undergoes more extensive DNA demethylation than the ICM and to evaluate whether naive hESCs resemble the demethylation observed in human germline, we performed whole-genome bisulfite sequencing (WGBS) of the human prenatal germline genome to create a comprehensive single-base resolution map

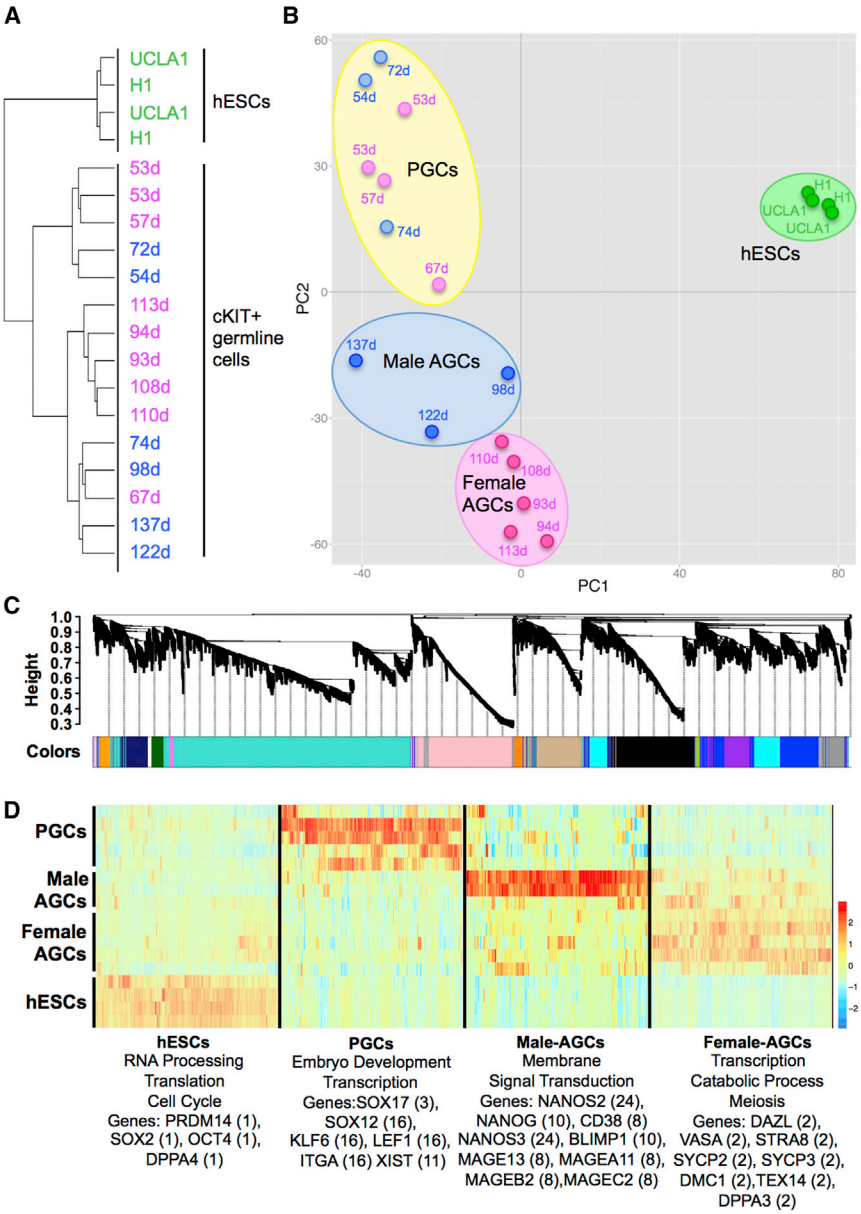

Figure 1. Human Germ Cells Are Distinct from hESCs

(A) Unsupervised hierarchical clustering of hESCs and cKIT-expressing germline cells isolated from human prenatal testes (blue) or ovaries (pink). Day (d) of prenatal development post-fertilization is shown.

(B) PCA. Each dot represents a sample. Blue, male; pink, female germline cells; green, hESCs. Germline samples separate into three clusters in PC2, including PGCs and AGCs, which are either male or female.

(C) Weighted gene co-expression network analysis of hESC, PGC, and AGC samples showing a hierarchical cluster tree of co-expression modules. Each module corresponds to a branch labeled by a distinct color shown underneath.

(D) Heatmap showing relative expression of 6,583 genes in 4 representative modules across all samples. For each developmental window, only the most highly correlated modules are shown with assigned biological names: hESCs (module 1), PGCs (module 16), male AGCs (module 24), and female AGCs (module 2). Representative gene ontology terms enriched in the highest correlated module are shown below, as well as representative hESC and germ cell-related genes found in the statistically significant modules for that group. The specific module is shown in parentheses.

See also Figure S1.

of DNA demethylation dynamics of human prenatal germline cells. This resource is critical not only for understanding the resetting of epialleles prior to birth in vivo but also for measuring genome-wide DNA methylation reprogramming in in vitro systems such as the generation of hESCs in the naive ground state.

RESULTS

We began by establishing transcriptional landmarks of human prenatal germline development using RNA sequencing (RNA-seq) of purified germ cells from n = 9 ovaries and n = 6 testes from 53 to 137 days of life post-fertilization. Human germline cells were isolated from individual ovaries and testes using fluorescence activated cell sorting (FACS) for the surface receptor cKIT (Figure S1A). No pooling of samples was performed for this study. We have previously shown that germline cells sorted using this strategy are 100% pure by single-cell RT-PCR (Gkountela et al., 2013). Here, we confirmed the purity of human germline samples using an expanded panel of germ-cell-expressed genes on single cells, including *SOX17*, which was positive in almost every *BLIMP1*, *NANOS3* double-positive cell (Figure S1B).

RNA-seq of 15 human prenatal germline samples yielded 633 million trimmed 50bp reads, with almost 500 million reads uniquely mapped to the human genome (Table S1). RNA-seq was also performed on equivalent numbers of TRA-1-81-sorted primed hESCs called UCLA1 (n = 2) and H1 (n = 2). Using unsupervised hierarchical clustering, as well as principle component analysis (PCA), we discovered that all human cKIT-positive germline cells clustered separately from TRA-1-81-positive hESCs (Figures 1A and 1B and Table S4). We note that one female sample (67 days) clustered with the male cKIT sorted germline cells in unsupervised hierarchical clustering (Figure 1A), yet clustered together with the younger germline group composed of male and female germline cells in PCA (Figure 1B). Similarly, we also found that the 74 day male germline cells clustered with the older male germline group in unsupervised hierarchical clustering, but with the younger group in PCA. Therefore, we speculate that, at around 67 days in females and 74 days in males, the germline cells are transitioning

between the younger and older stages. Given the distinct clustering in PC2 (Figure 1B), we will refer to the germline cells in the top quadrant as PGCs and the germline cells in the bottom quadrant as male or female advanced germline cells (AGCs).

In order to understand the relationships between PGCs and male and female AGCs, we performed a weighted gene co-expression network analysis (WGCNA) (Langfelder and Horvath, 2008). This is an unbiased, unsupervised analysis that identifies co-expression modules corresponding to clusters of co-expressed transcripts in each group. We identified 39 modules of co-expressed transcripts with 11 modules significant to PGCs, 5 modules significant to male AGCs, and 14 modules significant to female AGCs (Figures 1C, 1D, and S1C and Table S4). In the PGC-specific modules, we identified RNAs associated with embryonic lineage development, including *SOX17*, the newest transcription factor implicated in human PGC specification (Irie et al., 2015), as well as other embryonic transcription factors such as *SRY-box-12* (*SOX12*), *Kruppel-like factor 6* (*KLF6*), and *lymphoid enhancer binding factor 1* (*LEF1*). In the AGC-specific modules, we identified meiotic genes such as *synaptonemal protein complex 2* (*SYCP2*), *SYCP3*, *Stimulated by retinoic acid 8* (*STRA8*), and *DMC1* in female AGCs. In male AGCs, the significantly enriched modules included genes such as *NANOS2*, *NANOG*, *CD38*, *NANOS3*, *PRDM1* and a variety of cancer/testis antigens (Figure 1D). We performed a pairwise comparison of RNA expression between PGCs and AGCs and found a significant enrichment in genes associated with reproductive processes and genome defense in AGCs relative to PGCs (Figures S1D, S1E, and S1G). We also discovered RNAs associated with meiosis and ovarian folliculogenesis that were specific to female AGCs (Figure S1F). A surprise was the expression of *XIST* in a module significant to PGCs and not female AGCs. The RNA-seq analysis confirmed that *XIST* RNA was present in both male and female PGCs, as well as male and female AGCs (Figure S1H). These results demonstrate that, in the germline, *XIST* expression is not restricted to females.

Given that the PGC-specific modules identified enrichment of genes involved in embryo development genes rather than typical "reproductive genes," we hypothesized that human PGCs may resemble an "indifferent" cell type, such as ICM cells or naive ground state hESCs, with the reproductive program becoming dominant after the progression to AGCs. To investigate this, we performed PCA comparing TRA-1-81-sorted primed hESCs (H1 and UCLA1), H9 primed and H9 naive ground state hESCs (Takashima et al., 2014), and ICM cells isolated from human blastocysts (Yan et al., 2013). We discovered that human germline cells clustered as a single group, distinct from ICM cells, as well as hESCs in either the primed or the naive ground state (Figure S1I). Given the unique transcriptional identity of human germline cells and the discovery that the human germline can be developmentally grouped into distinct clusters of either PGCs or AGCs, we next quantified DNA methylation in the human germline using these developmental landmarks as guides.

DNA methylation was evaluated in the human germline using WGBS from n = 4 pairs of ovaries and n = 2 pairs of testes. All analyses were performed on cytosines with $\geq$ 3 reads per cytosine (Table S2). Three libraries corresponded to the PGC stage, 57 days (female), 59 days (male), and 67 days (female), and three libraries corresponded to the AGC stage, 113 days (n = 2 females) and 137 days (male). The bisulfite conversion efficiency estimated from Lambda DNA spike-in was the following: CG = 99.4%; CHG = 98.3%; and CHH = 99.2%. We also compared our human prenatal germline data to previously published WGBS datasets of H1, H9, and HSF1 hESCs (Laurent et al., 2010; Lister et al., 2011; Chen et al., 2011); human ICM and human embryonic liver (Guo et al., 2014); and naive ground state hESCs (called H9 naive) and the parental H9 hESC line used for reversion (called H9 primed) (Takashima et al., 2014).

The average percent of CpG methylation estimated from our libraries revealed that the human prenatal germline contains the lowest genome-wide average for CpG methylation reported in a human genome to date, with the 113 day female AGCs containing an average of 16.7% CpG methylation. The naive ground state hESCs were higher at 29.2%, and the ICM was 40.03% (Figure 2A). In 137 day male AGCs, the average CpG methylation was quantified as being 41.5%, whereas the average CpG methylation in the 59 day male PGCs was 30.7%, indicating that, between 59 and 137 days of development in males, the genome initiates de novo methylation. An overview of the bulk CpG methylation level for all samples is available in Figure S2A.

Next, we evaluated the distribution of DNA methylation at individual cytosines by plotting cytosine methylation in 10% increments as a fraction of total methylation from 0–1 (0%–100%) (Figures 2B, S2B, and S2C). In the ICM (Figure 2B), PGCs, embryonic liver, and male AGCs (Figures S2B and S2C), the distribution of CpG methylation is bimodal, whereas in the most demethylated 113 day female germline sample, the majority of CpGs (> 0.6) are hypomethylated (0%–20% methylation) (Figure 2B). Similarly, with reversion of H9 primed hESCs to the naive ground state, a large fraction of cytosines also become hypomethylated; however, an equally large fraction of cytosines exhibit intermediate levels of DNA methylation (21%–79%) (Figure 2B). Given that the female germline cells were progressively demethylating from 57 to 113 days of development, whereas the male germline cells have initiated de novo methylation, we focused on the female germline cells for the reminder of the study.

By merging reads from the two female PGC libraries and the two female AGC libraries to increase depth, we plotted CpG methylation across entire genome and discovered that methylation is globally lost along entire chromosomes in PGCs, and this is further reduced in AGCs. In this analysis, we discovered that naive hESCs resemble the genome-wide level of PGCs, but not the ICM (Figure 2C). The metagene plot of CpG methylation revealed a drop of CpG methylation around transcription start sites (TSSs) in all samples (Figure 2D), with AGCs averaging the lowest level of CpG methylation in the gene body and upstream and downstream regions, followed by PGCs and naive hESCs (Figure 2D). In all three cases (AGCs, PGCs, and naive hESCs), CpG methylation at reference genes was lower than the ICM (Figure 2D). The metaplot of CpG islands (CGIs) revealed low levels of methylation in all cell types; however, both PGCs and AGCs show extremely low methylation compared to ICM and naive hESCs (Figure 2E). Given that CpG methylation is severely depleted at CGIs in the germline, we plotted percent CpG methylation relative to CpG density and discovered that

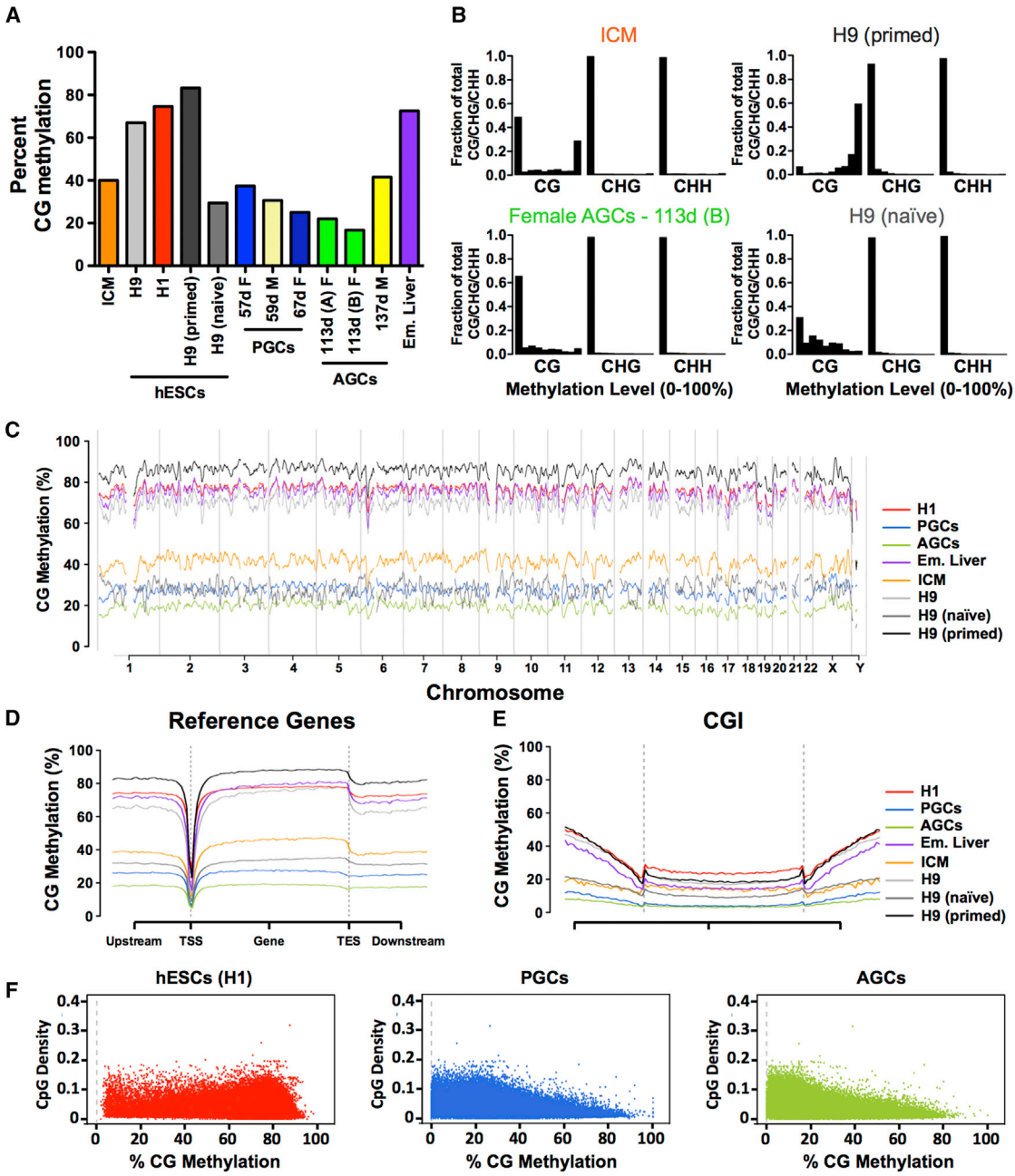

Figure 2. Female AGCs Represent the Most Demethylated Genomic State

(A) Average CpG methylation in human ICM, hESCs, PGCs, AGCs, and embryonic liver (Em. Liver). Age of male (M) and female (F) germline samples in days (d) postfertilization is shown.

(B) Distribution of cytosine methylation in ICM and AGCs and H9 primed and H9 naive hESCs. The x axis represents methylation levels binned in ten increments of 10% (i.e., 0%–10%, 10%–20%, etc.). y axis is the fraction of total CG/CHG/CHH.

(C) Average genome-wide levels of CpG methylation across all chromosomes in 1 Mb windows. PGCs, merged reads from 57 and 67 day germline cells; AGCs, merged reads from 113 day germline cells; H9 primed and H9 naïve, merged reads from 3 biological replicates.

(D) Metaplot of CpG methylation at reference genes. TSS, transcription start site; TES, transcription end site.

(E) Metaplot of CpG methylation at CGI.

(F) Correlation between CpG density and methylation for H1 hESCs; PGCs (merged) and AGCs (merged). PGCs, AGCs, Em. (Embryonic), and ICM.

See also Figure S2.

cytosines with >80% CpG methylation in PGCs and AGCs are generally located in regions of low CpG density (Figure 2F).

In order to evaluate CpG methylation reprogramming in vivo, we generated boxplots of cytosine methylation in 5 kb windows and evaluated the fate of hypermethylated (≥80%) and hypomethylated (≤20%) windows common to ICM and germline cells (Figures 3A and 3B). We also evaluated these same parameters in primed hESCs and embryonic liver, where DNA methylation levels are consistently high (Figures S3A and S3B). The purpose of this analysis was to determine whether highly methylated cytosines in ICM are erased in the germline and vice versa. In general, our results show that hypermethylated windows in the ICM (n = 8,850) are hypomethylated in PGCs and AGCs. Conversely, hypermethylated windows in PGCs and AGCs (n = 21) generally retain some methylation in the ICM (Figure 3A). Analysis of hypomethylated windows in ICM and germline cells reveals similarly low methylation levels in both cell types (Figure 3B). This is in contrast to hESCs and embryonic liver, which on average maintained highly methylated cytosines at these windows. Taken together, these data demonstrate that the most hypermethylated windows of the ICM exhibit demethylation in the germline, whereas hypermethylated germline windows are only partially demethylated in the ICM. Therefore, methylation reprogramming in vivo involves greater reliance on the germline.

In order to identify regions of variable methylation in ICM, PGCs, and AGCs, we evaluated methylation in 5 kb windows common to the datasets shown (n = 565,299) (Figures 3C and S3C). As expected, we discovered that most methylation variable regions in ICM, PGCs, and AGCs were hypomethylated relative to embryonic liver and primed hESCs. However, we also identified variable regions that were more methylated in AGCs than in PGCs (Figure S3C). To probe this further, we calculated statistically significant ($p < 0.05$) differentially methylated regions (DMRs) with a >80% methylation difference in 200 bp windows (n = 1,049,420 windows analyzed total). This analysis yielded 3,445 DMRs between PGCs and AGCs, with a false discovery rate of < 0.001% (Figure 3D). We discovered that 3,255 DMRs lose methylation (94.5%) and 190 DMRs (5.5%) gain methylation in AGCs relative to PGCs. The hypomethylated DMRs were associated with 1,899 genes, and the hypermethylated DMRs were associated with 118 genes (Table S4). Analysis of intragenic genomic features containing hypo- and hypermethylated DMRs revealed particular enrichment at DMR-containing CGIs located within exons, splice sites, promoters, and 3′ UTRs (Figures 3E and 3F). We also evaluated cytosine methylation at imprinting control centers (ICCs) for two paternally methylated imprinted genes, *H19* and *MEG3*, and two maternally methylated imprinted genes, *PEG3* and *KCNQ1* (Figure S3D). Our results show that, consistent with previous data (Gkountela et al., 2013), there is an almost complete loss of cytosine methylation at ICCs in AGCs relative to PGCs.

In order to determine whether DMRs between PGCs and AGCs correlated with changes in gene expression, we compared the RNA-seq of female germline cells at the equivalent ages to the germline cells used for WGBS (Figure 3G). This comparison revealed 12 DMR-associated genes that were also differentially expressed. All 12 genes were hypomethylated in AGCs relative to PGCs, and 2/12 were associated with meiosis (*TEX14* and *SYCE2*). Taken together, our data reveal a remarkable and pervasive loss of DNA methylation in human PGCs and AGCs during prenatal life that has almost no relationship to changes in gene expression. Our results unexpectedly show that the female germline undergoes locus-specific changes in intragenic DNA methylation at exons, splice sites, and promoters, as well as small amounts of de novo methylation in the background of a demethylated genome.

Given these dynamic changes in the human germline, we also re-examined CpG methylation in the mouse germline (Seisenberger et al., 2012). We remapped the dataset to the mm9 mouse genome, with all analyses performed on cytosines with ≥3 reads per cytosine (Table S3). Similar to the human study, we mapped methylation 5 kb windows common to the dataset shown (n = 499,541) and identified variably methylated regions (Figure 3H). We found that the female mouse germline also undergoes modest gains in cytosine methylation, particularly between E13.5 and E16.5 (Figure 3H), which can be quantified as an increase from 4.68% at E13.5 to 9.13% at E16.5 (Figure S3E). The hypo- and hyper-methylated DMRs between female germline cells at E13.5 and E16.5 revealed particular enrichment at CGI-containing DMRs in exons, splice sites, promoters, and 3′UTRs (Figure S3G). These are the same intragenic regions exhibiting DMRs in the human germline between PGCs and AGCs.

Given that the human germline does not demethylate by 113 days of life to the epigenetic ground-state levels quantified for the mouse genome at E13.5, we hypothesized that some regions of the genome are resistant to demethylation, therefore persisting in the globally demethylated genome. To identify these sites, we evaluated common 200 bp windows in ICM, PGCs, and AGCs containing at least 6 CpG sites (n = 67,817 windows). Using a cutoff of ≥50% average CpG methylation in each 200 bp window, we identified 1,471 persistently methylated regions in all three samples (Figure 3I). Analysis of genomic features containing persistent methylation identified enrichment, particularly at exons. CGI-containing persistent regions exhibited a further enrichment at exons, as well as in 3′UTRs, promoters, and splice sites (Figure 3I). To identify genes associated with persistently methylated regions, we used the genomic regions enrichment of annotations tool (GREAT) (McLean et al., 2010). We restricted our analysis to the identification of genes with persistent methylation within gene bodies or ± 5kb of the TSS. This uncovered 585 genes (Table S4). These genes are not necessarily repressed in PGCs and represent diverse mechanisms, including chromatin remodeling (*SETDB1*, *SETD1A*, *UHRF1*, and *Chromodomain helicase 6* [*CHD6*]), cell adhesion (*CDH4* and *CDH12*), and map kinase signaling (*MAPK8* and *MAPK10*).

In the mouse germline, persistently methylated regions are associated with murine-specific endogenous retroviruses (ERV) known as intracisternal particle A (IAP) (Rebollo et al., 2012). IAP sequences do not exist in the human genome; therefore, we evaluated DNA demethylation at ERVs, as well as LINEs. For this analysis, we evaluated methylation in the human germline cells, as well as hESCs (naive and primed), ICM, and embryonic liver. Our results show that demethylation of all transposons as an aggregate follows the trend for the genome average (Figure 4A). Some specific examples include *HERVK*, *HERV1*,

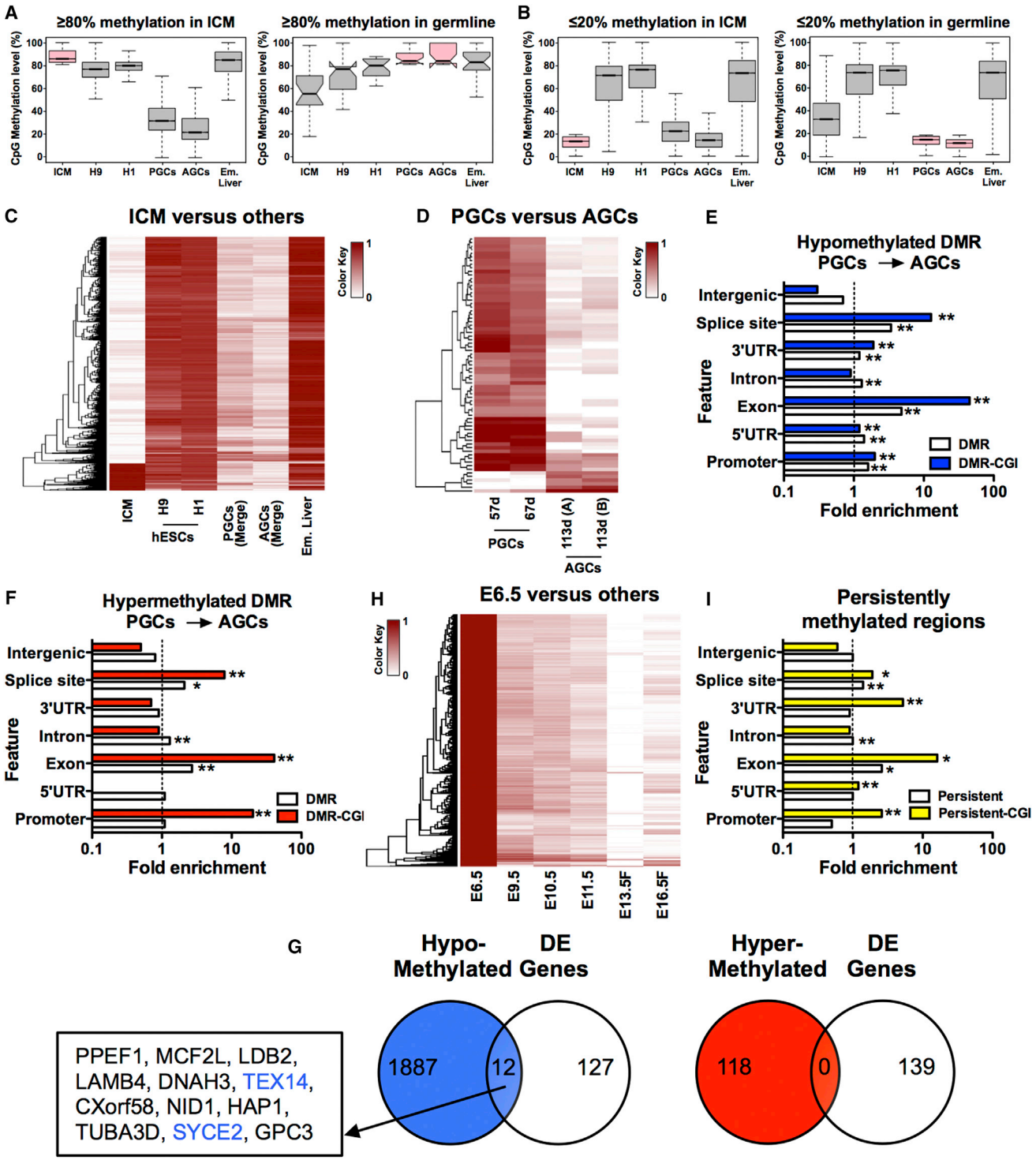

Figure 3. Methylation Reprogramming In Vivo Is Dynamic in Human and Mouse

(A) Boxplots showing fate of highly methylated CpGs (≥80% CpG methylation) in ICM (left) and germline cells (right). For ICM, n = 8,850 hypermethylated windows of 5 kb were identified. For PGC and AGC, we identified n = 21 hypermethylated 5 kb windows.

(B) Boxplots showing hypomethylated windows (<20% CpG methylation) in ICM (left) and germline cells (right). For ICM, n = 64,787 windows, and for germline cells n = 95,479 5 kb windows were identified.

(C) Heatmaps showing methylation variable regions in 5 kb windows with >80% methylation difference in ICM (n = 9,072, FDR = 2.28%) relative to other samples.

(D) Heatmap of differentially methylated regions between PGCs and AGCs using 200 bp windows (n = 1,049,420) with 3,456 DMRs (3,445 merged DMRs) (FDR < 0.001%) identified (0.33% of the total number of windows).

(legend continued on next page)

HERVL, *LINE 2* (*L2*), *L3*, and *L4* (Figures S4A–S4C). However, we were able to identify unique methylation differences among ICM, germline cells, and naive hESCs when the repetitive elements were classified into subfamilies. For example, *HERVK9-Int* and *HERVK11-Int* subfamilies showed persistent methylation in ICM, PGCs, and AGCs and pronounced demethylation in the H9 naive cells (Figure 4B). Additional transposons that showed pronounced demethylation in the H9 naive hESCs relative to ICM and germline cells are the L1 class of transposons (Figure 4C). For example, we found relatively high DNA methylation levels across the transposon body of young L1 *Homo sapiens* specific (*L1HS*), as well as the immediate descendants *L1PA2* and *L1PA3* in ICM and in germline cells. However, in the H9 naive cells, CpG methylation was the lowest of all cell types with a pronounced hypomethylated valley at the 5′ end of *L1HS* and *L1PA2*. The hypomethylated valley was almost completely resolved by the next descendant *L1PA3*, yet even by L1PA8, the H9 naive hESCs still have the lowest levels of methylation at this transposon subclass relative to the other cell types. This suggests that reversion of H9 hESCs to the naive state leads to efficient targeting (or failed protection) of this transposon family for demethylation (Figure 4C).

Despite these dynamic changes in DNA methylation at specific transposon subclasses, the median expression of all transposons is low (FPKM less than 1.0), and in most cases, the highest expressing transposons of each subclass (the transposons in the upper quartiles of expression) are reduced between PGCs and AGCs (as shown for *HERVK*), and similarly are reduced between primed and naive hESCs (as shown for *HERVK*, *L1HS*, and *L1PA*) (Figure 4D). Previous studies revealed that increased *HERVH* expression is associated with the naive state (Wang et al., 2014b), and consistent with this, we find that the upper quartiles of *HERVH* expression are greater in the naive hESCs relative to the primed state (Figure S4D). A similar example in the germline is the expression of *L1HS*, where both the median and upper quartiles of *L1HS* expression are higher in AGCs relative to PGCs (Figure 4D). Although *L1HS* tends to be hypermethylated in the germline relative to the genome average for PGCs and AGCs (Figure 4C), the median CpG methylation for *L1HS* is lower in AGCs relative to PGCs (Figure 4E). Similarly for *HERVH*, CpG methylation at this transposon subclass is reduced in naive hESCs relative to primed, which is consistent with the increase in expression (Figure S4D). However, these examples, although important, appear to be exceptions to the rule, as the majority of transposons exhibit no change or lower expression in the more demethylated cell types (Figure 4E).

Given the highly demethylated state in human germline cells from 57–113 days of development, we examined the RNA-seq dataset for clues to the mechanisms that may maintain DNA hypomethylation in the germline. We found that RNAs encoding *DNA methyltransferase 1* (*DNMT1*), its co-factor *UHRF1*, and the de novo methyltransferases *DNMT3A*, *DNMT3B*, and *DNMT3L* are all expressed in human germline cells (Figure 5A). This is different to the mouse germline where *Uhrf1*, *Dnmt3a*, and *Dnmt3b* RNAs are repressed (Kurimoto et al., 2008). Using immunofluorescence, we discovered that, despite detectable levels of RNAs, the UHRF1 and DNMT3A proteins are below the limit of detection in the majority of germline cells of both sexes, whereas hESCs express both proteins (Figures 5B–5G and 5I). This indicates that the maintenance and de novo methylation machinery are largely disabled in the human germline. Furthermore, we discovered that *TET CYTOSINE DIOXYGENASE 1* (*TET1*), *TET2*, and *TET3* are all expressed by human germline cells, with *TET1* RNA increasing as male and female PGCs progress to AGCs (Figure 5H).

In mouse germline cells, loss of DNA methylation is accompanied by a global loss of histone H3 lysine 9 dimethylation (H3K9me2) (Hajkova et al., 2008). The RNA-seq analysis revealed that the enzymes responsible for H3K9me2 and H3K9me3 (*EHMT2* and *SETDB1*, *SUV39H1*, and *SUV39H2*) are all expressed in PGCs and AGCs (Figure 5A). However, using immunofluorescence, we discovered that H3K9me2 is depleted from PGCs and is subsequently found in AGCs in a punctate pattern. In contrast, H3K9me3 is localized in a punctate pattern in the human germline at all stages of development (Figures S5B–S5E). Global loss of DNA methylation and H3K9me2 in mouse PGCs occurs downstream of *Prdm14* (Yamaji et al., 2008). Using immunofluorescence, we found that PRDM14 protein is localized to the nucleus of human PGCs (Figure S5A), although the RNA levels of *PRDM14* are very low compared to undifferentiated hESCs (Figure 5A). Taken together, the human germline at 57 days of development is extremely demethylated, has disabled its DNA methylation machinery, and has increased expression of *TET1*. Furthermore, we show that H3K9me3 is a stable silencing mark that can be identified in the germline at all stages of development.

DISCUSSION

The human germline and pre-implantation embryos are excellent in vivo models for quantifying both global and local sites of DNA demethylation and identifying loci that escape demethylation during nuclear reprogramming (Guo et al., 2014; Smith et al., 2014). In the human germline, global demethylation leads to a dramatic loss of almost all CGI methylation, which is consistent with the finding that persistently methylated cytosines tend to

(E and F) (E) Enrichment analysis of hypomethylated DMRs and (F) hypermethylated DMRs at indicated genomic features. Enrichment is accepted if fold enrichment is $\geq$1.0. DMRs and CGI-containing DMRs (DMR-CGI) are shown. *p < 0.05 and **p < 0.01.

(G) Correlation of hypo- (left) and hyper-methylated (right) DMRs with differentially expressed (DE) genes reveals limited to no overlap.

(H) Heatmaps showing methylation-variable regions in 5 kb windows with >80% methylation difference in E6.5 mouse epiblast (n = 499,541 total, variable n = 2,515) FDR = 0.1%. Female (F).

(I) Identification of genomic features with persistent methylation ($\geq$50% CpG methylation in 200 bp windows with > 6 CpG sites per window). n = 67,817 windows meeting this criteria were in common between datasets resulting in the identification of n = 1,471 persistently methylated windows (2.17%). For (C) (D), and (H), darker color indicates higher CpG methylation, and white indicates absence of CpG methylation. FDR, false discovery rate estimated from simulated methylomes (see Experimental Procedures).

See also Figure S3.

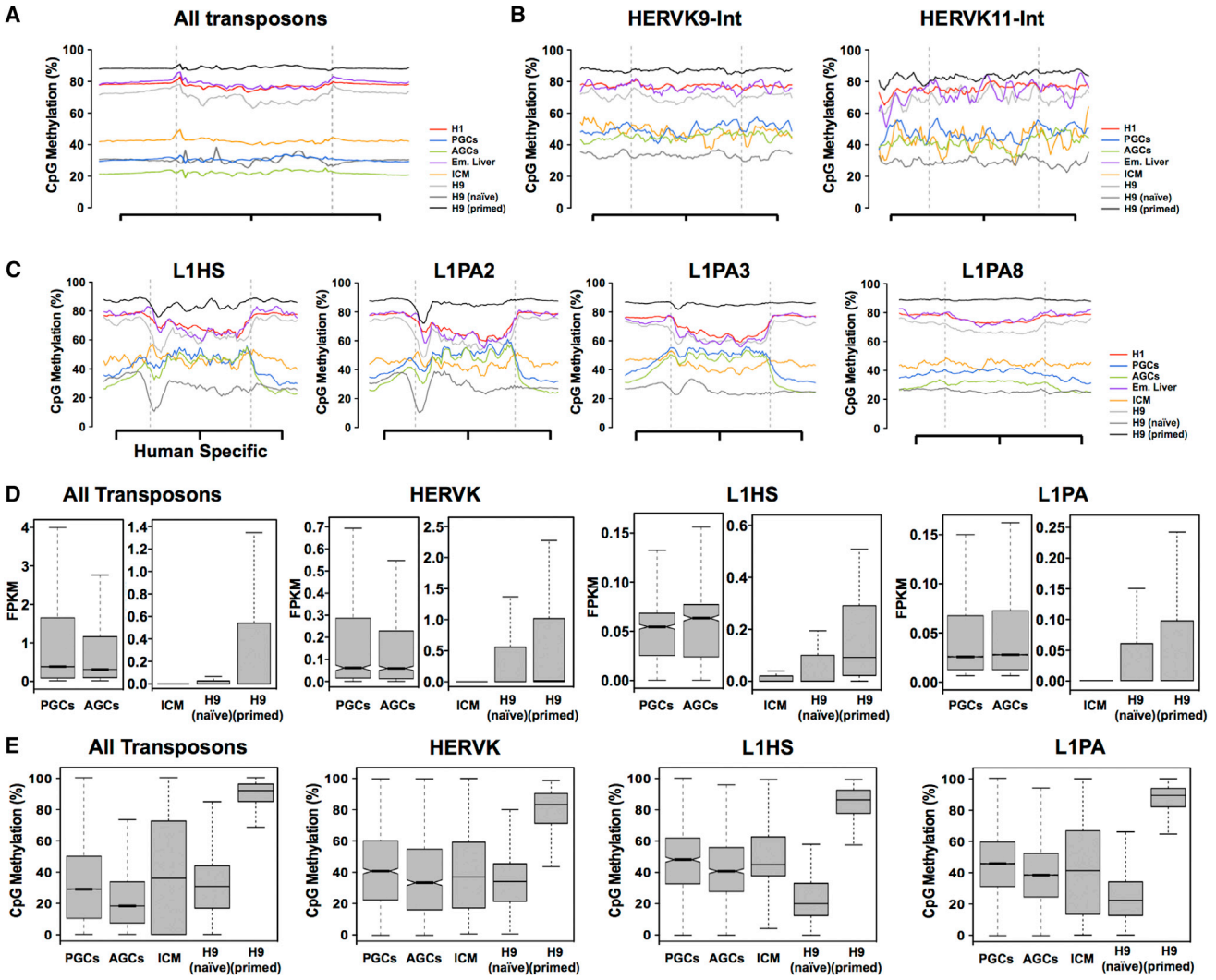

Figure 4. Demethylation of Transposable Elements in Naive hESCs In Vitro Is Less Restrained Than Germline Cells and ICM

(A) Metaplot of all transposons irrespective of type exhibit DNA demethylation similar to the genome average.

(B) Metaplots of CpG methylation across *HERVK9-int* and *HERK11-int* retrotransposons, showing that CpG methylation in PGCs and AGCs is comparable to ICM with H9 naive cells exhibiting the lowest levels of CpG methylation.

(C) Metaplots of CpG methylation for *L1HS*, *L1PA2*, *L1P3*, and *L1PA8*. Naive hESCs exhibit the lowest levels of CpG methylation at this subfamily (area within the dashed gray line). This is particularly dramatic at the younger elements such as the *Homo-sapiens*-specific *L1HS* and the closely related *L1PA2*.

(D) Boxplots showing average RNA expression of transposons in PGCs, AGCs, ICM, H9 naïve, and H9 primed hESCs as indicated. Average transposon expression is less than 1.0 FPKM.

(E) Boxplots showing CpG methylation of all transposons, *HERVK*, *L1HS*, and *L1PA* elements in PGCs, AGCs, ICM, and H9 naive and H9 primed hESCs.

See also Figure S4.

occur in regions of low CpG density, making WGBS a critical approach for identifying these sites. Furthermore, loss of CpG methylation in general does not correlate with gene expression changes in the germline. Instead, the RNA-seq reference map suggests that a common germline program distinguishes germline cells from other closely related demethylated cell types such as the ICM and naive hESCs, which is independent of the methylated state.

Recently, it was found that *SOX17* is required for human PGC specification (Irie et al., 2015). We also show that human germline cells are enriched in *SOX17* in the PGCs stage. However, based upon the expression of developmental transcription modules, we propose that PGC identity involves a relatively indifferent germline program that gives way to the expression of the sex-specific germline program upon transition to the advanced germline state, between 67 and 93 days in females and between 74 and 98 days in males. Similar to the mouse, we show that activation of the mature germline program does not depend solely on DNA demethylation but rather relies on additional genome-wide epigenetic reprogramming events. Recently, we showed that loss of H3K27me3 (Gkountela et al., 2013) is one such major epigenetic event in the human germline

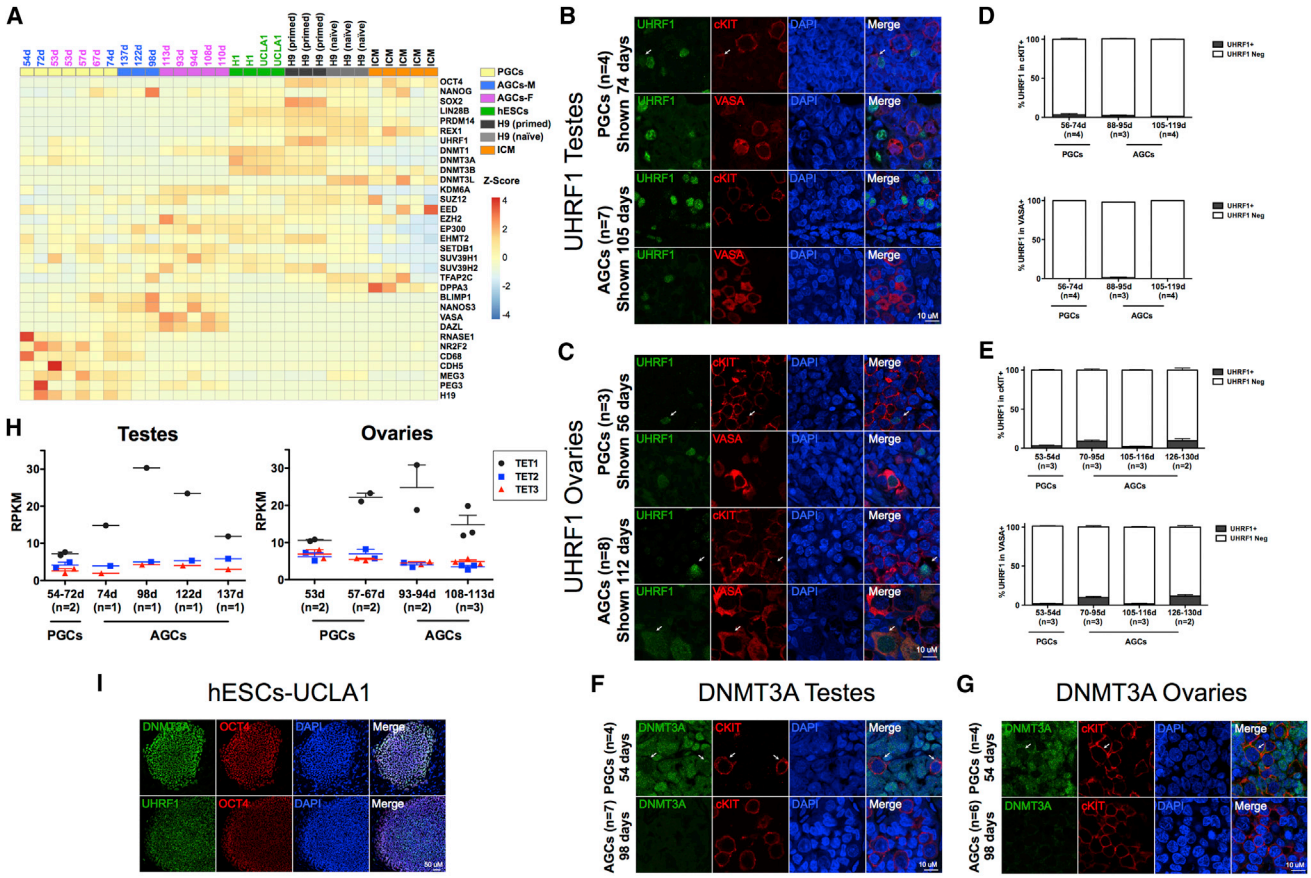

Figure 5. Protein Expression of UHRF1 and DNMT3A in Human Germline

(A) Heatmap showing normalized expression of indicated genes in PGCs, AGCs, hESCs, H9 primed, H9 naïve, and ICM. M, male; F, Female.

Note that *DNMT3L* is enriched in the H9 naive cells relative to the rest of the datasets, whereas *SOX2* and *UHRF1* are enriched in H9 primed cells.

(B, C, F, G, and I) Representative immunofluorescence micrographs of UHRF1 (B, C, and I) and DNMT3A (F, G, and I) with germline markers cKIT or VASA in prenatal testes (B and F) and ovaries (C and G) at the developmental stage indicated in days and with pluripotency marker OCT4 in UCLA1 hESCs (I). Arrows indicate UHRF1 or DNMT3A signal.

(D and E) Quantification of UHRF1 in cKIT+ or VASA+ germ cells in testes (D) and ovaries (E) at the developmental ages indicated days (d).

(D) In testes for quantification in cKIT+, 14 optic fields were counted at the PGC stage from n = 4 testes. For the AGC stage, 23 optic fields were counted from n = 3 testes at 87–95 days and 28 optic fields from n = 4 testes at 105–119 days of development. For quantification in VASA+, 12 optic fields were counted at the PGC stage from n = 4 testes. For the AGC stage, 22 optic fields were counted from n = 3 testes at 87–95 days, and 25 optic fields from n = 4 testes were counted at 105–119 days of development.

(E) In ovaries for quantification in cKIT+, 14 optic fields were counted at the PGC stage from n = 3 ovaries. For the AGC stage, 13 optic fields were counted from n = 3 ovaries at 70–95 days, 9 optic fields from n = 3 ovaries at 105–116 days, and 8 optic fields from n = 2 ovaries at 126–130 days of development. For quantification in VASA+, 13 optic fields were counted at the PGC stage from n = 3 ovaries. For the AGC stage, 15 optic fields were counted from n = 3 ovaries at 70–95 days, 8 optic fields from n = 3 ovaries at 105–116 days, and 8 optic fields from n = 2 ovaries at 126–130 days of development.

(H) Expression levels of TET1-3 in prenatal testes and ovaries from 53 days to 137 days (n= number of samples at each developmental stage). For immunofluorescence microscopy, nuclei were counterstained with DAPI (blue). Scale bars, 10 um. In (D), (E), and (H), data are represented as mean ± SEM. Days (d), neg (negative).

See also Figure S5.

that is temporally linked to the transcriptional transition of PGCs to AGCs reported in this study. Based on our germline methylome analysis, we propose that global hypomethylation, as well as depletion of H3K9me2 during the PGC stage, sets the epigenetic stage for germline sex-specific maturity, with loss of H3K27me3 allowing differentiation to the advanced stages. Notably, *XIST* non-coding RNA is expressed in both male and female germline at all stages, even before global loss of H3K27me3 from the nucleus, indicating that *XIST* may be non-silencing in the germline, similar to what was reported for human blastomeres (Okamoto et al., 2011). Future work using fluorescence in situ hybridization for X-linked genes, together with single-cell imaging, will be required to confirm whether *XIST* is indeed expressed from both X chromosomes and whether, similar to mouse, human female PGCs begin with an inactive X that subsequently undergoes X reactivation.

In mice, PGCs are specified from brachyury-positive cells emerging through the primitive streak (Aramaki et al., 2013). In

contrast, *sox17/SOX17* is considered a marker of definitive endoderm and hemogenic endothelium in the mouse and human (Choi et al., 2012; D'Amour et al., 2005; Nakajima-Takagi et al., 2013). This raises a critical question as to the germ layer origin of PGCs in humans. Our data support the hypothesis that the human germline is not set aside in the ICM of human blastocysts, as the transcriptome and methylome of PGCs are distinct from ICM. Instead, our data show that the transcriptome of germline cells (but not the methylome) is closer to primed hESCs relative to hESCs in the naive state or ICM. Human ESCs do not exist in the embryo (they are in vitro cell types); therefore, the closer transcriptional relationship of germline cells to primed hESCs may be due to expression of RNAs involved in embryo development (Takashima et al., 2014). In future studies, our reference map of the human germline transcriptome can be used to uncover the transcriptional relationship between human PGCs and the earliest germ layers in order to address this question.

In the current study, we used the RNA-seq and WGBS data of naive hESCs cultured in t2iL+Go (Takashima et al., 2014). However, there are multiple approaches for generating naive hESCs beginning with the first report using naive human stem cell media (NHSM) to the more recent media called 5i/L/FA (Gafni et al., 2013; Chan et al., 2013; Valamehr et al., 2014; Ware et al., 2014; Takashima et al., 2014; Theunissen et al., 2014). PCA of the published transcriptomes indicates that all approaches generate naive cell types slightly different from each other, with 5iL/FA closest to t2iL+Go (Theunissen et al., 2014). We focused on the t2iL+Go naive hESCs for our study because it was the only dataset to include both WGBS and RNA-seq on the same sequencing platform. Our results indicate that reversion to the naive state in t2iL+Go creates an in vitro cell type that is more demethylated compared to the ICM it is hypothesized to represent. We found that a consistent occurrence in this media was the unbridled demethylation at young L1 transposable elements *L1HS* and *L1PA2*. The more restrained demethylation at these features in ICM and germline suggests that the mechanisms either targeting or preventing demethylation at these discreet sites are different in vivo relative to reversion in vitro. Alternatively, the *HERV* expression pattern in the naive hESCs and especially the elevated *HERVH* family levels could serve as a cellular identity marker in naive hESCs, essential for safeguarding self-renewal (Wang et al., 2014a; Göke et al., 2015). In future studies, it will be critical to determine whether the other naive medias, or reversion of other cell types in the same media, acquire a similar demethylated state as H9 in t2iL+Go. We show that our reference map of human germline cells combined with the work in the human pre-implantation embryo will be critical for interpreting future reversion strategies to the naive state.

Global demethylation at transposable elements in general does not lead to transcriptional activation, raising an important question as to the mechanisms by which active transposons are silenced in the human germline during prenatal life, given the depletion of repressive chromatin marks such as H3K9me2 and H3K27me3 (Gkountela et al., 2013). The finding that *L1HS* transposons are highly methylated at all stages of germline development relative to the older and extinct *L1PA* ancestors could indicate that methylation is employed as a first line of defense by the germline for the transcriptional repression of *L1HS*. This is supported by the finding that a small decrease in methylation between PGCs and AGCs is associated with a median increase in *L1HS* expression in AGCs. One purpose for the maintained DNA methylation at young potentially active transposons could be to facilitate C-T mutations and transposon extinction. In support of this, extinct *L1PA* ancestors have progressively fewer CpG nucleotides as a result of C-T conversion than the younger active elements (Walser et al., 2008). Alternatively, active transposons that escape demethylation may impact silencing of surrounding genomic regions leading to positional effects in vivo. The primed to naive reversion and ultralow methylation at the 5′end of *L1HS* could be used as a tractable model to test this.

In the current study, we did not distinguish between 5mC and 5hmC in the human germline genome. In the mouse germline, 5mC is rapidly oxidized to 5hmC in a very discreet window between E10.5 to E12.5 (Hackett et al., 2013), which is now referred to as stage II germline DNA demethylation (reviewed by Lee et al., 2014; Vincent et al., 2013; Yamaguchi et al., 2013). In contrast, stage I DNA demethylation (which occurs from E7.5 to E9.5) removes around 50% of methylated CpGs from the genome using a Tet-independent mechanism (Vincent et al., 2013). Given that the human germline has already completed stage I DNA demethylation by 57 days of life (the equivalent of E9.5 in mice), we hypothesize that the removal of DNA methylation between 57 and 113 days also involves oxidation to 5hmC at discreet loci. Indeed, in previous studies, we could simultaneously identify both 5mC and 5hmC during DNA demethylation (Gkountela et al., 2013), indicating that conversion of 5mC to 5hmC is heterogeneous both at individual loci and also at individual cells within a gonad. Given that we continue to see DNA demethylation from 67 to 113 days, our study suggests that stage II demethylation in humans takes months (rather than days) and that re-methylation at discreet genomic features occurs before demethylation is complete. Notably, the small amount of re-methylation in female mouse germline cells between E13.5 and E16.5 at intragenic CGI-containing DMRs is conserved in humans. However, unlike mice, it temporally overlaps with the final stages of demethylation. Therefore, given the protracted stage II demethylation in the human germline relative to the mouse, the analysis of 5hmC in future studies should involve analysis of 5hmC and 5mC in the same gonad or alternatively single-cell 5hmC analysis within the one gonad when the technology becomes available.

Taken together, the RNA-seq and WGBS reference maps of the human germline described here provide a critical reference for in vivo DNA demethylation beyond the methylated state attained in the human blastocyst (Guo et al., 2014; Smith et al., 2014). Specifically, we have identified methylated regions in the human germline that are targeted for deeper demethylation in H9 naive hESCs, suggesting that these transposons should be carefully monitored in naive hESC cultures with extended culture. We also discovered dynamic locus-specific maintenance and de novo DNA methylation in a background of extreme global genome demethylation, a phenomenon also reported in human embryos in which a number of loci are seen to escape DNA demethylation (Smith et al., 2014). Thus, global DNA demethylation is a complex process in which global and local mechanisms work together to shape the epigenome.

EXPERIMENTAL PROCEDURES

RNA-Seq Data Analysis

Differential gene expression analysis was performed using the packages DESeq (Anders and Huber, 2010) and edgeR (Robinson et al., 2010) in R (http://www.R-project.org). Raw read counts (GEO accession number GSE63392) were used and modeled based on a negative binomial distribution. We filtered out genes with RPKM < 1 in both groups. The multiple testing errors were corrected by the false discovery rate (FDR). In addition to the FDR of < 0.05, we considered differentially expressed genes as having >2-fold difference. Thus, in summary, we considered genes as differentially expressed if (1) the FDR was less than 0.05; (2) the expression ratio between two time points was >2×; (3) the maximal RPKM value for at least one group in the comparison was >1; and (4) there was agreement between DESeq and edgeR. See also the Supplemental Experimental Procedures.

Weighted Gene Co-expression Network Analysis

To understand which gene networks determine gene expression difference between cell populations at a systems level, we performed WGCNA (Langfelder and Horvath, 2008). This unsupervised and unbiased analysis identified distinct co-expression modules by clustering transcripts with the similar expression pattern across samples. To further understand the cell population specificity of the modules, we correlated the identified module eigengenes with traits represented as the theoretical expression patterns for all cell populations in a binary fashion.

Genome-wide DNA Methylation Profiles

The raw data have been deposited to GEO (accession number GSE63392). Bisulfite converted reads were aligned to the reference genome (hg19) using BS Seeker 2 (Guo et al., 2013). Genome-wide DNA methylation profiles were generated by determining methylation levels for each cytosine in the genome. Because bisulfite treatment converts unmethylated cytosines (Cs) to thymines (Ts) after PCR amplification, the methylation level at each cytosine was estimated as #C/(#C+#T), where #C is the number of methylated reads and #T is the number of unmethylated reads. The methylation level per cytosine serves as an estimate of the percentage of cells that have a methylated cytosine at a specific locus. We only included cytosines that are covered by at least three reads. The resulting methylation profiles from germ cells covered up to 77% of the cytosines genome wide (see Table S2).

ACCESSION NUMBERS

The accession numbers for the raw data reported in this paper are GEO: GSE63392 and GEO: GSE63393.

SUPPLEMENTAL INFORMATION

Supplemental Information includes Supplemental Experimental Procedures, five figures, and four tables and can be found with this article online at http://dx.doi.org/10.1016/j.cell.2015.05.012.

AUTHOR CONTRIBUTIONS

S.G. performed experiments and data interpretation and wrote manuscript; K.X.Z. performed RNA-seq data analysis; T.A.S. performed immunofluorescence staining; W.-W.L. performed WGBS data analysis; J.H.-C. performed confocal microscopy; P.-Y.C. designed and performed the RNA-seq, WGBS data analysis, and interpretation and wrote the manuscript; and A.T.C. conceived experiments, performed data analysis, and wrote the manuscript.

ACKNOWLEDGMENTS

The authors would like to thank the UCLA BSCRC flow cytometry core for flow and FACS assistance and BSCRC High Throughput Sequencing core. This work was supported by grants from the NIH (NIH/NICHD HD058047 and NIH/NICHD HD079546) awarded to A.T.C., as well as the Eli and Edythe Broad Center of Regenerative Medicine and Stem Cell Research and by grants from Academia Sinica and National Health Research Institutes, Taiwan (NHRI-EXI03-10324SC) to P.-Y.C. We would also like to acknowledge the support of the California Institute for Regenerative Medicine (CIRM) Predoctoral training grant (TG2-01169) for funding J.H.-C.

Received: November 14, 2014
Revised: February 13, 2015
Accepted: March 25, 2015
Published: May 21, 2015

REFERENCES

Anders, S., and Huber, W. (2010). Differential expression analysis for sequence count data. Genome Biol. *11*, R106.

Aramaki, S., Hayashi, K., Kurimoto, K., Ohta, H., Yabuta, Y., Iwanari, H., Mochizuki, Y., Hamakubo, T., Kato, Y., Shirahige, K., and Saitou, M. (2013). A mesodermal factor, T, specifies mouse germ cell fate by directly activating germline determinants. Dev. Cell *27*, 516–529.

Chan, Y.S., Göke, J., Ng, J.H., Lu, X., Gonzales, K.A., Tan, C.P., Tng, W.Q., Hong, Z.Z., Lim, Y.S., and Ng, H.H. (2013). Induction of a human pluripotent state with distinct regulatory circuitry that resembles preimplantation epiblast. Cell Stem Cell *13*, 663–675.

Chen, P.Y., Feng, S., Joo, J.W., Jacobsen, S.E., and Pellegrini, M. (2011). A comparative analysis of DNA methylation across human embryonic stem cell lines. Genome Biol. *12*, R62.

Choi, E., Kraus, M.R., Lemaire, L.A., Yoshimoto, M., Vemula, S., Potter, L.A., Manduchi, E., Stoeckert, C.J., Jr., Grapin-Botton, A., and Magnuson, M.A. (2012). Dual lineage-specific expression of Sox17 during mouse embryogenesis. Stem Cells *30*, 2297–2308.

D'Amour, K.A., Agulnick, A.D., Eliazer, S., Kelly, O.G., Kroon, E., and Baetge, E.E. (2005). Efficient differentiation of human embryonic stem cells to definitive endoderm. Nat. Biotechnol. *23*, 1534–1541.

Ficz, G., Hore, T.A., Santos, F., Lee, H.J., Dean, W., Arand, J., Krueger, F., Oxley, D., Paul, Y.L., Walter, J., et al. (2013). FGF signaling inhibition in ESCs drives rapid genome-wide demethylation to the epigenetic ground state of pluripotency. Cell Stem Cell *13*, 351–359.

Gafni, O., Weinberger, L., Mansour, A.A., Manor, Y.S., Chomsky, E., Ben-Yosef, D., Kalma, Y., Viukov, S., Maza, I., Zviran, A., et al. (2013). Derivation of novel human ground state naive pluripotent stem cells. Nature *504*, 282–286.

Gkountela, S., Li, Z., Vincent, J.J., Zhang, K.X., Chen, A., Pellegrini, M., and Clark, A.T. (2013). The ontogeny of cKIT+ human primordial germ cells proves to be a resource for human germ line reprogramming, imprint erasure and in vitro differentiation. Nat. Cell Biol. *15*, 113–122.

Göke, J., Lu, X., Chan, Y.S., Ng, H.H., Ly, L.H., Sachs, F., and Szczerbinska, I. (2015). Dynamic transcription of distinct classes of endogenous retroviral elements marks specific populations of early human embryonic cells. Cell Stem Cell *16*, 135–141.

Guo, W., Fiziev, P., Yan, W., Cokus, S., Sun, X., Zhang, M.Q., Chen, P.Y., and Pellegrini, M. (2013). BS-Seeker2: a versatile aligning pipeline for bisulfite sequencing data. BMC Genomics *14*, 774.

Guo, H., Zhu, P., Yan, L., Li, R., Hu, B., Lian, Y., Yan, J., Ren, X., Lin, S., Li, J., et al. (2014). The DNA methylation landscape of human early embryos. Nature *511*, 606–610.

Habibi, E., Brinkman, A.B., Arand, J., Kroeze, L.I., Kerstens, H.H., Matarese, F., Lepikhov, K., Gut, M., Brun-Heath, I., Hubner, N.C., et al. (2013). Whole-genome bisulfite sequencing of two distinct interconvertible DNA methylomes of mouse embryonic stem cells. Cell Stem Cell *13*, 360–369.

Hackett, J.A., Sengupta, R., Zylicz, J.J., Murakami, K., Lee, C., Down, T.A., and Surani, M.A. (2013). Germline DNA demethylation dynamics and imprint erasure through 5-hydroxymethylcytosine. Science *339*, 448–452.

Hajkova, P. (2011). Epigenetic reprogramming in the germline: towards the ground state of the epigenome. Philos. Trans. R. Soc. Lond. B Biol. Sci. *366*, 2266–2273.

Hajkova, P., Ancelin, K., Waldmann, T., Lacoste, N., Lange, U.C., Cesari, F., Lee, C., Almouzni, G., Schneider, R., and Surani, M.A. (2008). Chromatin dynamics during epigenetic reprogramming in the mouse germ line. Nature *452*, 877–881.

Heard, E., and Martienssen, R.A. (2014). Transgenerational epigenetic inheritance: myths and mechanisms. Cell *157*, 95–109.

Irie, N., Weinberger, L., Tang, W.W., Kobayashi, T., Viukov, S., Manor, Y.S., Dietmann, S., Hanna, J.H., and Surani, M.A. (2015). SOX17 is a critical specifier of human primordial germ cell fate. Cell *160*, 253–268.

Kobayashi, H., Sakurai, T., Miura, F., Imai, M., Mochiduki, K., Yanagisawa, E., Sakashita, A., Wakai, T., Suzuki, Y., Ito, T., et al. (2013). High-resolution DNA methylome analysis of primordial germ cells identifies gender-specific reprogramming in mice. Genome Res. *23*, 616–627.

Kurimoto, K., Yabuta, Y., Ohinata, Y., Shigeta, M., Yamanaka, K., and Saitou, M. (2008). Complex genome-wide transcription dynamics orchestrated by Blimp1 for the specification of the germ cell lineage in mice. Genes Dev. *22*, 1617–1635.

Langfelder, P., and Horvath, S. (2008). WGCNA: an R package for weighted correlation network analysis. BMC Bioinformatics *9*, 559.

Laurent, L., Wong, E., Li, G., Huynh, T., Tsirigos, A., Ong, C.T., Low, H.M., Kin Sung, K.W., Rigoutsos, I., Loring, J., and Wei, C.L. (2010). Dynamic changes in the human methylome during differentiation. Genome Res. *20*, 320–331.

Lee, H.J., Hore, T.A., and Reik, W. (2014). Reprogramming the methylome: erasing memory and creating diversity. Cell Stem Cell *14*, 710–719.

Lister, R., Pelizzola, M., Kida, Y.S., Hawkins, R.D., Nery, J.R., Hon, G., Antosiewicz-Bourget, J., O'Malley, R., Castanon, R., Klugman, S., et al. (2011). Hotspots of aberrant epigenomic reprogramming in human induced pluripotent stem cells. Nature *471*, 68–73.

McLean, C.Y., Bristor, D., Hiller, M., Clarke, S.L., Schaar, B.T., Lowe, C.B., Wenger, A.M., and Bejerano, G. (2010). GREAT improves functional interpretation of cis-regulatory regions. Nat. Biotechnol. *28*, 495–501.

Nakajima-Takagi, Y., Osawa, M., Oshima, M., Takagi, H., Miyagi, S., Endoh, M., Endo, T.A., Takayama, N., Eto, K., Toyoda, T., et al. (2013). Role of SOX17 in hematopoietic development from human embryonic stem cells. Blood *121*, 447–458.

Okamoto, I., Patrat, C., Thépot, D., Peynot, N., Fauque, P., Daniel, N., Diabangouaya, P., Wolf, J.P., Renard, J.P., Duranthon, V., and Heard, E. (2011). Eutherian mammals use diverse strategies to initiate X-chromosome inactivation during development. Nature *472*, 370–374.

Rebollo, R., Miceli-Royer, K., Zhang, Y., Farivar, S., Gagnier, L., and Mager, D.L. (2012). Epigenetic interplay between mouse endogenous retroviruses and host genes. Genome Biol. *13*, R89.

Robinson, M.D., McCarthy, D.J., and Smyth, G.K. (2010). edgeR: a Bioconductor package for differential expression analysis of digital gene expression data. Bioinformatics *26*, 139–140.

Seisenberger, S., Andrews, S., Krueger, F., Arand, J., Walter, J., Santos, F., Popp, C., Thienpont, B., Dean, W., and Reik, W. (2012). The dynamics of genome-wide DNA methylation reprogramming in mouse primordial germ cells. Mol. Cell *48*, 849–862.

Smith, Z.D., Chan, M.M., Humm, K.C., Karnik, R., Mekhoubad, S., Regev, A., Eggan, K., and Meissner, A. (2014). DNA methylation dynamics of the human preimplantation embryo. Nature *511*, 611–615.

Takashima, Y., Guo, G., Loos, R., Nichols, J., Ficz, G., Krueger, F., Oxley, D., Santos, F., Clarke, J., Mansfield, W., et al. (2014). Resetting transcription factor control circuitry toward ground-state pluripotency in human. Cell *158*, 1254–1269.

Theunissen, T.W., Powell, B.E., Wang, H., Mitalipova, M., Faddah, D.A., Reddy, J., Fan, Z.P., Maetzel, D., Ganz, K., Shi, L., Lungjangwa, T., et al. (2014). Systematic identification of culture conditions for induction and maintenance of naive human pluripotency. Cell Stem Cell *15*, 471–487.

Valamehr, B., Robinson, M., Abujarour, R., Rezner, B., Vranceanu, F., Le, T., Medcalf, A., Lee, T.T., Fitch, M., Robbins, D., and Flynn, P. (2014). Platform for induction and maintenance of transgene-free hiPSCs resembling ground state pluripotent stem cells. Stem Cell Reports *2*, 366–381.

Vincent, J.J., Huang, Y., Chen, P.Y., Feng, S., Calvopiña, J.H., Nee, K., Lee, S.A., Le, T., Yoon, A.J., Faull, K., et al. (2013). Stage-specific roles for tet1 and tet2 in DNA demethylation in primordial germ cells. Cell Stem Cell *12*, 470–478.

Walser, J.C., Ponger, L., and Furano, A.V. (2008). CpG dinucleotides and the mutation rate of non-CpG DNA. Genome Res. *18*, 1403–1414.

Wang, J., Xie, G., Singh, M., Ghanbarian, A.T., Raskó, T., Szvetnik, A., Cai, H., Besser, D., Prigione, A., Fuchs, N.V., et al. (2014a). Primate-specific endogenous retrovirus-driven transcription defines naive-like stem cells. Nature *516*, 405–409.

Wang, L., Zhang, J., Duan, J., Gao, X., Zhu, W., Lu, X., Yang, L., Zhang, J., Li, G., Ci, W., et al. (2014b). Programming and inheritance of parental DNA methylomes in mammals. Cell *157*, 979–991.

Ware, C.B., Nelson, A.M., Mecham, B., Hesson, J., Zhou, W., Jonlin, E.C., Jimenez-Caliani, A.J., Deng, X., Cavanaugh, C., Cook, S., et al. (2014). Derivation of naive human embryonic stem cells. Proc. Natl. Acad. Sci. USA *111*, 4484–4489.

Yamaguchi, S., Hong, K., Liu, R., Inoue, A., Shen, L., Zhang, K., and Zhang, Y. (2013). Dynamics of 5-methylcytosine and 5-hydroxymethylcytosine during germ cell reprogramming. Cell Res. *23*, 329–339.

Yamaji, M., Seki, Y., Kurimoto, K., Yabuta, Y., Yuasa, M., Shigeta, M., Yamanaka, K., Ohinata, Y., and Saitou, M. (2008). Critical function of Prdm14 for the establishment of the germ cell lineage in mice. Nat. Genet. *40*, 1016–1022.

Yan, L., Yang, M., Guo, H., Yang, L., Wu, J., Li, R., Liu, P., Lian, Y., Zheng, X., Yan, J., et al. (2013). Single-cell RNA-Seq profiling of human preimplantation embryos and embryonic stem cells. Nat. Struct. Mol. Biol. *20*, 1131–1139.